Highly Efficient and Selective Hydrogenation of Nitroaromatics on Photoactivated Rutile Titanium Dioxide

Yasuhiro Shiraishi,*,[†] Yoshiki Togawa,[†] Daijiro Tsukamoto,[†] Shunsuke Tanaka,[‡] and Takayuki Hirai[†]

[†]Research Center for Solar Energy Chemistry, and Division of Chemical Engineering, Graduate School of Engineering Science, Osaka University, Toyonaka 560-8531, Japan

[‡]Department of Chemical, Energy and Environmental Engineering, Kansai University, Suita 564-8680, Japan

S *Supporting Information*

ABSTRACT: We report that photoactivated rutile titanium dioxide (TiO_2) catalyzes a highly efficient and selective hydrogenation of nitroaromatics with alcohol as a hydrogen source. Photoirradiation (λ >300 nm) of rutile TiO_2 suspended in alcohol containing nitroaromatics at room temperature and atmospheric pressure produces the corresponding anilines with almost quantitative yields, whereas common anatase and P25 TiO_2 show poor activity and selectivity. The Ti^{3+} atoms located at the oxygen vacancies on the rutile surface behave as the adsorption site for nitro-

aromatics and the trapping site for photoformed conduction band electrons. These effects facilitate rapid and selective nitro-to-amine hydrogenation of the adsorbed nitroaromatics by the surface-trapped electrons, enabling aniline formation with significantly high quantum yields (>25% at <370 nm). The rutile TiO_2 system also facilitates chemoselective hydrogenation of nitroaromatics with reducible substituents; several kinds of functionalized anilines are successfully produced with >94% yields.

KEYWORDS: *photocatalysis, titanium dioxide, rutile, nitroaromatics, hydrogenation*
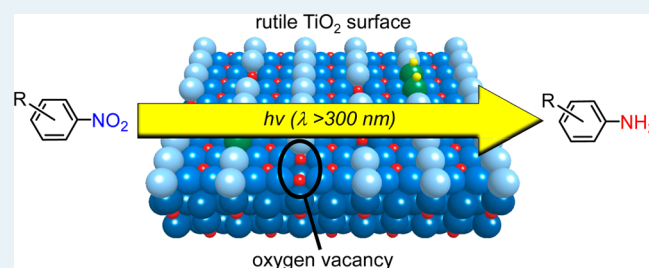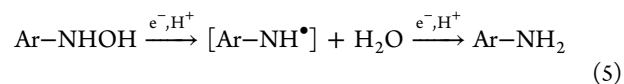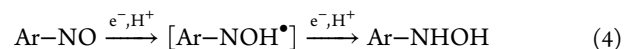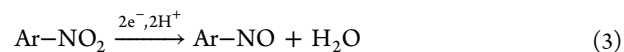
INTRODUCTION

Functionalized anilines are industrially important intermediates for the synthesis of pharmaceuticals, polymers, herbicides, and fine chemicals.[1] These compounds are generally produced by hydrogenation of nitroaromatics using stoichiometric or excess amounts of reducing agents, with a concomitant formation of copious amount of wastes.[2] Catalytic hydrogenation is therefore an ideal process; however, conventional platinum-group metal catalysts with molecular hydrogen (H_2) as a hydrogen source promote hydrogenation of other functionalities such as vinyl and carbonyl groups and results in poor selectivity.[3] Several catalytic systems have been proposed so far, but only a few systems have succeeded selective nitro hydrogenation.[4−9] The most efficient systems employ gold nanoparticles supported on TiO_2 or Fe_2O_3,[6−8] and silver nanoparticles covered with CeO_2 nanoparticles.[9] These systems successfully promote selective nitro hydrogenation, but require high H_2 pressure (>5 bar) and high temperature (>373 K). Alternative catalytic processes that promote selective nitro hydrogenation under milder reaction conditions are necessary for safe and clean synthesis of functionalized anilines.

Semiconductor titanium dioxide (TiO_2), activated by irradiation of ultraviolet (UV) light, promotes oxidation and reduction reactions at atmospheric pressure and room temperature, and has widely been used for decomposition of organic pollutants.[10] Application of TiO_2 photocatalysis to organic synthesis has also been studied. The reactions are, however, usually nonselective; selective transformations of

reactants to targeted products are difficult to achieve,[11,12] although recent studies reported some successful examples.[13−16] Photocatalytic hydrogenation of nitroaromatics with TiO_2 has also been studied with alcohol as a hydrogen source.[17−23] These reactions are performed by UV irradiation of TiO_2 suspended in alcohol containing nitroaromatics under inert gas atmosphere. Photoexcited TiO_2 produces the electron (e^-) and positive hole (h^+) pairs (eq 1). The h^+ oxidizes alcohol and produces ketone and protons (eq 2).[24] The reduction of nitroaromatics by e^- produces the corresponding anilines (eqs 3−5), via a formation of nitrosobenzene (Ar−NO) and *N*-phenylhydroxylamine (Ar−NHOH) intermediates.

$$TiO_2 + h\nu \rightarrow h^+ + e^- \tag{1}$$

$$(CH_3)_2CHOH \xrightarrow{2h^+} (CH_3)_2CO + 2H^+ \tag{2}$$

$$Ar-NO_2 \xrightarrow{2e^-,2H^+} Ar-NO + H_2O \tag{3}$$

$$Ar-NO \xrightarrow{e^-,H^+} [Ar-NOH^{\bullet}] \xrightarrow{e^-,H^+} Ar-NHOH \tag{4}$$

$$Ar-NHOH \xrightarrow{e^-,H^+} [Ar-NH^{\bullet}] + H_2O \xrightarrow{e^-,H^+} Ar-NH_2 \tag{5}$$

Table 1. Properties of TiO$_2$ Particles and Their Performance for Photocatalytic Hydrogenation of Nitrobenzene[a]
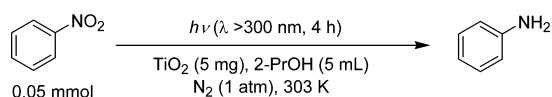
sample	catalyst	crystalline phase[b]	BET surface area/m^2 g^{-1}	particle size/ nm[c]	nitrobenzene conv./%[d]	aniline yield/ %[d]	aniline select./%	v_f[e]/μmol h^{-1}
1	JRC-TIO-1[f]	anatase	73	21	21	15	71	2.0
2	JRC-TIO-2[f]	anatase	18	400	13	4	31	0.9
3	ST-21[g]	anatase	67	25	23	6	26	0.9
4	ST-01[g]	anatase	217	7	37	27	73	
5	ST-41[g]	anatase	11	200	11	3	27	
6	HyCOM TiO$_2$[h]	anatase	132	13	16	8	50	
7	JRC-TIO-4 (P25)[f]	anatase 83%/rutile 17%	59	25	68	58	85	9.9
8	HF-treated P25[i]	rutile	32	71	>99	93	93	
9	PT-101[g]	rutile	25	71	>99	93	93	11.8
10	JRC-TIO-3[f]	rutile	40	41	>99	94	94	13.1
11	JRC-TIO-6[f]	rutile	100	17	>99	97	97	15.6
12	CR-EL[g]	rutile	7	250	>99	95	95	
13	NS-51[j]	rutile	7	220	>99	93	93	
14	Pt/JRC-TIO-6[k]	rutile			68	55	81	6.9
15	Ag/JRC-TIO-6[k]	rutile			86	75	87	
16	Pd/JRC-TIO-6[k]	rutile			92	76	83	
17	Au/JRC-TIO-6[k]	rutile			93	80	86	

[a]Photoirradiation was performed using a Xe lamp (2 kW; light intensity at 300−450 nm, 27.3 W m^{-2}). [b]Determined by XRD analysis (Figure S1, Supporting Information), where the anatase and rutile contents were determined with the equation: anatase (%) = $I_{anatase\ (101)}/(I_{anatase\ (101)} + 1.4 \times I_{rutile\ (110)}) \times 100$ (ref 29). [c]Determined by dynamic light scattering analysis. [d]Determined by GC. [e]Average initial rate for aniline formation, determined by dividing the amount of aniline formed during 2 h photoreaction by 2 (h). [f]Japan Reference Catalyst, supplied from the Catalyst Society of Japan. [g]Supplied from Ishihara Sangyo, Ltd. (Japan). [h]Prepared by hydrothermal crystallization in organic media (HyCOM) (ref 54). [i]Prepared by stirring P25 (1 g) in 10% HF (50 mL) for 24 h at room temperature followed by thorough washing with water. [j]Supplied from Toho Titanium Co., Ltd. (Japan). [k]Prepared by a photodeposition method (ref 24), where the metal loadings [= M/TiO$_2$ × 100] are Pt (0.57 wt %), Ag (0.55 wt %), Pd (0.50 wt %), and Au (0.30 wt %), respectively.

The overall reaction is expressed as follows:

$$Ar-NO_2 + 3(CH_3)_2CHOH$$
$$\rightarrow Ar-NH_2 + 3(CH_3)_2CO + 2H_2O \qquad (6)$$
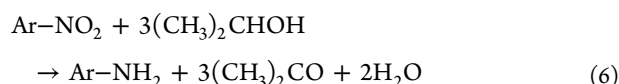
Selective production of aniline by TiO$_2$ photocatalysis is, however, significantly difficult. This is because, as shown by eqs 4 and 5, the nitrosobenzene and N-phenylhydroxylamine intermediates are converted to the reactive radicals ([Ar−NOH$^\bullet$] and [Ar−NH$^\bullet$]) by the reduction with e$^-$, and produce dimers (azobenzene and azoxybenzene) or polymerized materials.[25] Selective aniline production, therefore, requires rapid nitro-to-amine hydrogenation to suppress the side reactions promoted by the intermediates.

TiO$_2$ has three common polymorphic forms such as anatase, rutile, and brookite, and anatase and rutile forms are often employed for photocatalysis. Anatase usually shows much higher activity than rutile,[26] and its activity is further improved by coupling with about 20% rutile (Degussa P25 TiO$_2$).[27] Along these lines, early reported systems for photocatalytic nitro hydrogenation employed anatase or P25 TiO$_2$, resulting in insufficient activity and selectivity.[17−23]

Herein, we report that rutile TiO$_2$, which has been considered less active for photocatalysis, promotes nitro hydrogenation with significantly higher activity and selectivity than anatase and P25, enabling almost quantitative aniline production. IR, XPS, and UV−vis analysis revealed that the oxygen vacancy sites on the rutile surface behave as the active site facilitating rapid nitro-to-amine hydrogenation. Rutile TiO$_2$ also promotes chemoselective hydrogenation of nitroaromatics with reducible substituents, and successfully produce several kinds of functionalized anilines with >94% yields.

■ RESULTS AND DISCUSSION

The efficacy of rutile TiO$_2$ is evident from the hydrogenation of nitrobenzene in 2-PrOH using various kinds of anatase, P25, and rutile TiO$_2$ particles with different particle sizes and Brunauer−Emmett−Teller (BET) surface areas. Table 1 summarizes the nitrobenzene conversions and the aniline yields obtained by 4 h photoirradiation (λ >300 nm) of respective TiO$_2$ (5 mg) suspended in 2-PrOH (5 mL) containing nitrobenzene (10 mM) under N$_2$ atmosphere (1 atm). With anatase TiO$_2$ (samples **1−6**), the nitrobenzene conversions are <40% and the aniline selectivities are <75%. P25 TiO$_2$ (sample **7**) shows enhanced nitrobenzene conversion (68%), but the selectivity is still insufficient (85%). In these systems, GC and LC analysis of the solution detected azobenzene and azoxybenzene as major byproducts, and nitrosobenzene and N-phenylhydroxylamine as minor by-products (ca. 0.05 mM). These findings suggest that, as shown by eqs 4 and 5, the reactive radicals ([Ar−NOH$^\bullet$] and [Ar−NH$^\bullet$]) formed via the reduction of nitrosobenzene and N-phenylhydroxylamine intermediates indeed promote byproduct formation.[25] In contrast, rutile TiO$_2$ (samples **9−13**) promotes almost complete disappearance of nitrobenzene (>99%) and produces aniline with very high yields (>93%). During the reactions, neither nitrosobenzene nor N-phenylhydroxylamine was detected. These results clearly indicate that rutile TiO$_2$ rapidly promotes the nitro-to-amine hydrogenation sequence

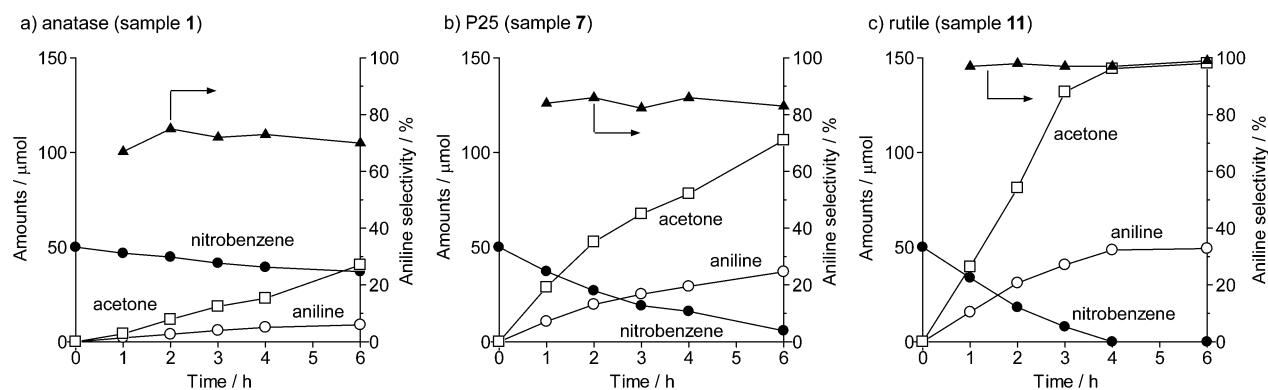a) anatase (sample **1**) b) P25 (sample **7**) c) rutile (sample **11**)

Figure 1. Time-dependent change in the amounts of substrate and products during photoreaction of nitrobenzene in 2-PrOH performed with (a) anatase (sample **1**), (b) P25 (sample **7**), or rutile TiO$_2$ (sample **11**). Reaction conditions are identical to those in Table 1.

(eqs 3–5). This suppresses side reactions and facilitates selective aniline production.

Figure 1 shows the time-dependent change in the amounts of substrate and products during photocatalytic reaction of nitrobenzene with respective anatase, P25, and rutile TiO$_2$. During photoirradiation, anatase and P25 show much lower nitrobenzene conversion and aniline selectivity than rutile. With rutile TiO$_2$, more than 4 h photoirradiation leads to complete transformation of nitrobenzene to aniline (50 μmol), along with a formation of almost three equivalents of acetone (150 μmol). H$_2$ gas was not detected during the reaction (detection limit: 0.1 μmol). This clearly indicates that the H atoms of alcohol, removed by oxidation with h$^+$ (eq 2), are consumed quantitatively by the nitro-to-amine hydrogenation (eqs 3–5), and stoichiometric oxidation and reduction reactions (eq 6) occur on the photoactivated rutile TiO$_2$.

As reported,[28] anatase TiO$_2$ dissolves in hydrofluoric acid (HF) more easily than rutile. Stirring P25 TiO$_2$ particles (1 g) in 10% HF solution (50 mL) for 24 h at room temperature followed by thorough washing with water successfully isolates pure rutile TiO$_2$, as evidenced by X-ray diffraction (XRD) analysis[29] (Figure S1, Supporting Information). As shown in Table 1 (sample **8**), the isolated rutile particles, when employed for photocatalytic hydrogenation of nitrobenzene, produce aniline with 93% yield, which is much higher than that obtained with P25 (58%, sample **7**). This clearly indicates that rutile TiO$_2$ indeed promotes rapid and selective nitro hydrogenation.

The active sites for nitro hydrogenation on rutile TiO$_2$ are the Ti^{3+} atoms located at the surface defects. As shown in Figure 2, the rutile (110) surface is characterized by alternate rows of 5-fold coordinated Ti^{4+} atoms and bridging O^{2-} atoms (O$_b$) that run in the (001) direction.[30] Surface defects are the O$_b$ vacancies, where two excess electrons associated with O$_b$ are transferred to the empty 3d orbitals of neighboring Ti^{4+} atoms, producing two Ti^{3+} atoms. These surface Ti^{3+} atoms behave as an adsorption site for nitroaromatics via an electron donation[31] and as a trapping site for photoformed conduction band e$^-$.[32] These two effects enable rapid nitro-to-amine hydrogenation on the surface Ti^{3+} atoms. The adsorption of nitroaromatics onto Ti^{3+} is confirmed by IR analysis. Figure 3a shows the IR spectra of nitrobenzene adsorbed onto the selected anatase or rutile TiO$_2$ particles in the gas phase. Two distinctive absorption bands appear at 1522 and 1346 cm^{-1}, which are assigned to asymmetric stretching vibration (ν_{asym}) of nitro group adsorbed on the surface Ti–OH group (Figure 2a) and symmetric stretching vibration (ν_{sym}) of nitro group adsorbed
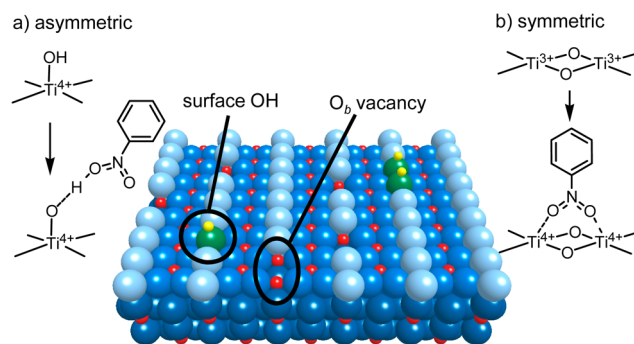
a) asymmetric b) symmetric

Figure 2. Surface structure of rutile TiO$_2$ (110), and (a) asymmetric and (b) symmetric adsorption modes of nitrobenzene. The light blue and green spheres are the O$_b$ atoms that lie in the [001] azimuth. The parallel red and yellow spheres are the Ti and H atoms, respectively.
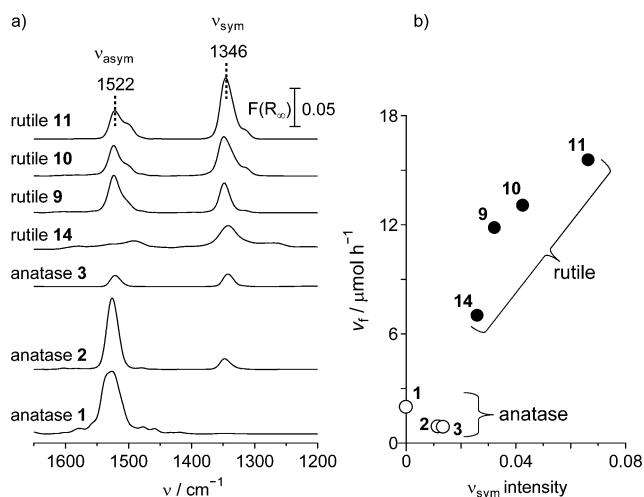

Figure 3. (a) Diffuse-reflectance IR spectra of nitrobenzene adsorbed on selected TiO$_2$ particles in the gas phase at 303 K. The numbers denote the catalysts listed in Table 1. The measurements were carried out as follows: TiO$_2$ (50 mg) was placed in an IR cell and evacuated (7.5 × 10^{-3} Torr) at 423 K for 3 h. Nitrobenzene (0.6 Torr) was introduced to the cell at 303 K, and the measurement was started. (b) Relationship between the ν_{sym} intensity and the average initial rate for aniline formation (ν_f) during photoreaction (2 h) of nitrobenzene on the respective TiO$_2$ (Table 1). The reaction conditions are identical to those in Table 1.

on the surface Ti^{3+} (Figure 2b), respectively.[33] The intensities of ν_{sym} band on the rutile TiO$_2$ particles (samples **9–11**) are

much stronger than those on anatase TiO_2 (samples **1–3**), because the rutile surface contains a larger number of O_b vacancy.[34,35] Figure 3b summarizes the relationship between the ν_{sym} intensity and the average initial rate for photocatalytic aniline formation (ν_f/μmol h^{-1}) on the respective catalysts, determined by 2 h photoreaction (Table 1). The obtained proportional relationship implies that nitroaromatics are adsorbed onto the surface Ti^{3+} atoms and undergo hydrogenation, and the number of surface Ti^{3+} atoms is the crucial factor for nitro hydrogenation.

The surface Ti^{3+} atoms as the active site for nitro hydrogenation is further confirmed by the loading of metal particles onto the TiO_2 surface by the conventional photodeposition method.[24] Photoirradiation of TiO_2 in an alcohol solution containing metal precursors successfully leads to a deposition of metal particles. Photoexcitation of the metal-loaded TiO_2 enables the migration of conduction band e$^-$ to the metal particles. This enhances charge separation between e$^-$ and h$^+$ pairs, and usually shows increased photocatalytic activity as compared to bare TiO_2.[36] Some literatures reported that anatase or P25 TiO_2 loaded with noble metal nanoparticles promotes photocatalytic reduction of nitroaromatics more efficiently than bare TiO_2, because of the enhanced charge separation.[21–23] However, as shown in Table 1 (samples **14–17**), the aniline yields obtained by rutile TiO_2 loaded with Pt, Ag, Pd, or Au particles (≤80%) are lower than those of pure rutile TiO_2 (97%, sample **11**). This suggests that reduction of nitrobenzene on the surface of metal particles by e$^-$ is inefficient as compared to that on the rutile surface. As shown in Figure 3a (sample **14**), the Pt-loaded rutile TiO_2 shows decreased ν_{sym} intensity as compared to pure rutile (sample **11**). This is because the Pt particles loaded on the rutile surface covers the Ti^{3+} atoms and suppresses the adsorption of nitrobenzene onto the Ti^{3+} atoms. In addition, as shown in Figure 3b, the data for sample **14** shows similar tendency to those for other rutile TiO_2 particles. These findings suggest that surface Ti^{3+} atoms indeed behave as the active site for nitro hydrogenation.

The adsorption of nitroaromatics onto the surface Ti^{3+} atoms occurs via the electron donation from Ti^{3+} to nitrobenzene. This is confirmed by X-ray photoelectron spectroscopy (XPS). As shown in Figure 4a, XPS chart for rutile TiO_2, treated in vacuo at elevated temperature, shows Ti $2p_{1/2}$ and $2p_{3/2}$ signals. These signals consist of two components assigned to Ti^{4+} (blue) and surface Ti^{3+} (red).[37] The mole fractions of these Ti components are determined by integration of the signals to be 92% and 8%, respectively. The mole fractions of the respective components are similar to those determined by scanning tunneling microscopy (STM) of rutile (110) surface (7 ± 3%).[35] In contrast, as shown in Figure 4b, the adsorption of nitrobenzene onto the sample creates an additional signal at higher binding energy (green), along with almost complete disappearance of the Ti^{3+} signal. The mole fraction of the new Ti component is determined to be 8%, which is similar to that of Ti^{3+} on pure rutile surface. This indicates that the surface Ti^{3+} are oxidized to Ti^{4+},[38] via the electron donation to the adsorbed nitrobenzene (Figure 2b).

The electron donation from surface Ti^{3+} atom to adsorbed nitrobenzene is further confirmed by UV–vis analysis. As shown in Figure 5a (solid line), the fundamental absorption edge of rutile TiO_2 is about 420 nm. Adsorption of nitrobenzene creates a red-shifted band (dotted line), although nitrobenzene itself absorbs light at <270 nm. This new band is
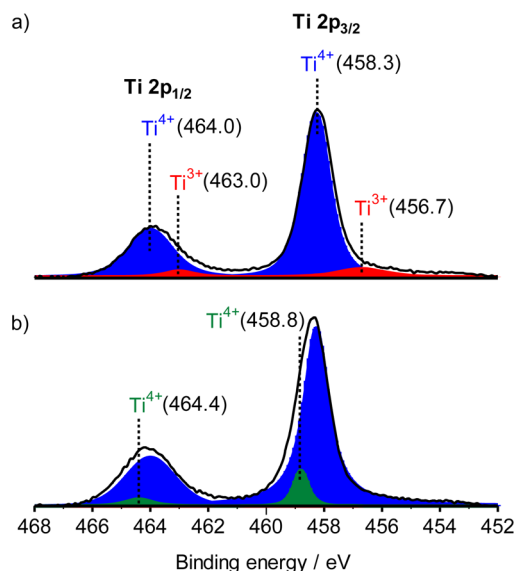

Figure 4. XPS chart (Ti 2p region) of (a) rutile TiO_2 (sample **11**) and (b) the sample after adsorption of nitrobenzene in the gas phase. The spectrum (a) was measured as follows: TiO_2 (50 mg) was evacuated (7.5×10^{-3} Torr) at 423 K for 3 h, and placed on a sample stage immediately to avoid the oxidation of Ti^{3+} by O_2. The sample was evacuated at room temperature for 6 h, and measurement was started. The spectrum (b) was obtained with the sample obtained after IR measurement (Figure 3a). The sample was evacuated at room temperature for 6 h, and measurement was started.
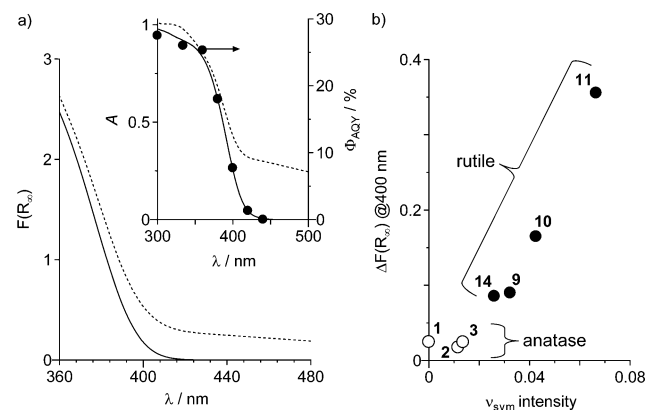

Figure 5. (a) Diffuse reflectance UV–vis spectra of (solid line) rutile TiO_2 (sample **11**) and (dotted line) the sample after adsorption of nitrobenzene in the gas phase. The spectrum for bare TiO_2 was obtained without pretreatment. Nitrobenzene-adsorbed samples were prepared in an IR cell (see the caption of Figure 3). The samples were moved to the UV–vis cell, and the measurement was started. (Inset) Absorption spectra of the samples and the apparent quantum yields for aniline formation [Φ_{AQY} (%) = (aniline formed ×6)/(photon number entering into the reaction vessel) × 100)] during photoreaction of nitrobenzene with rutile TiO_2 (sample **11**) at different light wavelengths. (b) Relationship between the intensity of differential spectrum at 400 nm ($\Delta F(R_\infty)$) and the ν_{sym} intensity for respective TiO_2 (Figure 3a). UV–vis spectra for other TiO_2 samples are summarized in Figure S3 (Supporting Information).

due to the interfacial charge transfer (IFCT)[39] from the TiO_2 valence band to the adsorbed nitrobenzene, as also observed for TiO_2 when loaded with Cu(II)[40] or Fe(III).[41] As shown in Figure 6, the edges of conduction band (E_{CB}) and valence band (E_{VB}) of rutile TiO_2 are located at 0 and 3.0 V (vs NHE, pH 0),
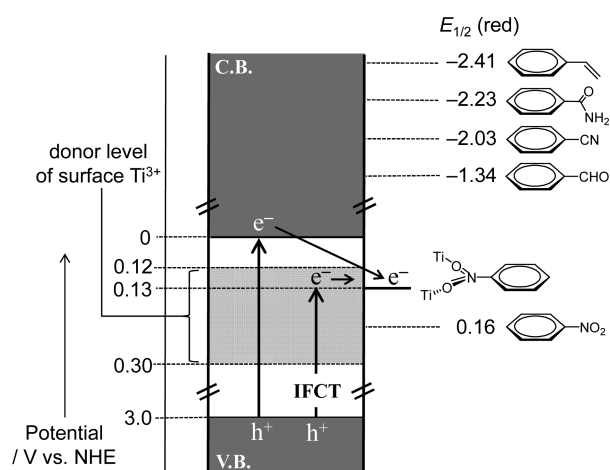
Figure 6. Energy diagram for rutile TiO$_2$ and half-wave reduction potentials of several benzene derivatives.

respectively. The energy of the observed CT transition is determined to be 2.87 eV (Figure S2, Supporting Information). The donor level of this transition (0.13 V) is more negative than the reduction potential of nitrobenzene (0.16 V).[42] This suggests that the red-shifted absorption is indeed due to the IFCT transition from the TiO$_2$ valence band to the adsorbed nitrobenzene. As reported,[43] the donor levels of surface Ti^{3+} atoms are located at 0.12–0.3 eV below E_{CB}. The donor level of the observed IFCT transition (0.13 V) is located within this range (Figure 6). This suggests that surface Ti^{3+} atoms strongly interact with the adsorbed nitrobenzene via the electron donation and, hence, facilitates IFCT transition from the TiO$_2$ valence band to nitrobenzene. As shown in Figure 5b, the plots of IFCT absorption at 400 nm versus the ν_{sym} intensity

obtained by IR analysis (Figure 3a) show proportional relationship. This again supports the electron donation from the surface Ti^{3+} atoms to the adsorbed nitrobenzene.

The closed keys in Figure 5a (inset) show the apparent quantum yield for aniline formation (Φ_{AQY}) determined by photocatalytic hydrogenation of nitrobenzene with rutile TiO$_2$ (sample **11**) using monochromatic lights at different wavelengths. The plots are almost consistent with the absorption spectrum of TiO$_2$. This clearly suggests that, as shown in Figure 6, the IFCT excitation scarcely contributes to the nitro hydrogenation, and the band gap photoexcitation of rutile TiO$_2$ and subsequent trapping of the conduction band e$^-$ by the surface Ti^{3+} atoms promote the nitro hydrogenation. As reported,[31] in the thermal decomposition of NO$_2$ gas on rutile TiO$_2$, the adsorption of NO$_2$ on the surface Ti^{3+} atoms significantly weakens the N–O bonds by the electron donation from Ti^{3+} and enhances decomposition. Similarly in the present photocatalytic system, strong adsorption of nitroaromatics onto the surface Ti^{3+} atoms probably weakens their N–O bonds and, hence, facilitates rapid nitro-to-amine hydrogenation. This is consistent with the activity of catalysts that depends on the amount of surface Ti^{3+} atoms (Figure 3b). It must be noted that, as shown in Figure 5a (inset), Φ_{AQY} values obtained by photoirradiation at <370 nm is >25%, which are much higher than the values for common photocatalytic reactions on bare TiO$_2$ (<10%).[44−46] This indicates that the present photocatalytic reaction proceeds very efficiently.

The proportional relationship between the ν_{sym} intensity and ν_f on rutile catalysts (samples **9−11**, Figure 3b) suggests that the number of surface Ti^{3+} atoms on the catalyst is the crucial factor for the activity of nitro hydrogenation. As shown in Table 1, BET surface areas of these three rutile TiO$_2$ catalysts are 25, 40, and 100 m^2 g^{-1}, respectively, indicating that the number of

Table 2. Photocatalytic Hydrogenation of Nitroaromatics on TiO$_2$[a]

entry	substrate	catalyst	solvent [b]	t / h [c]	substrate conv. / % [d]	product	product yield / % [d]
1 [e]	NO$_2$	JRC-TIO-6 (rutile **11**)	2-PrOH	6	>99	NH$_2$	>99
2 [e]		JRC-TIO-4 (P25 **7**)			88		74
3 [e]	NO$_2$	JRC-TIO-6 (rutile **11**)	2-PrOH/toluene (1/9 w/w)	4	>99	NH$_2$	98
4 [e]		JRC-TIO-4 (P25 **7**)			92		85
5	Cl—NO$_2$	JRC-TIO-6 (rutile **11**)	2-PrOH/toluene (1/9 w/w)	5	>99	Cl—NH$_2$	94
6		JRC-TIO-4 (P25 **7**)			>99		88
7	NO$_2$	JRC-TIO-6 (rutile **11**)	2-PrOH/toluene (9/1 w/w)	7	>99	NH$_2$	98
8		JRC-TIO-4 (P25 **7**)			71		55
9	H$_2$NOC—NO$_2$	JRC-TIO-6 (rutile **11**)	2-PrOH/THF (5/5 w/w)	6	>99	H$_2$NOC—NH$_2$	94
10		JRC-TIO-4 (P25 **7**)			58		35
11	NC—NO$_2$	JRC-TIO-6 (rutile **11**)	2-PrOH/toluene (1/9 w/w)	6	>99	NC—NH$_2$	97
12		JRC-TIO-4 (P25 **7**)			65		49
13 [f]	OHC—NO$_2$	JRC-TIO-6 (rutile **11**)	2-PrOH/toluene (1/9 w/w)	6	>99	OHC—NH$_2$	94
14 [f]		JRC-TIO-4 (P25 **7**)			62		36

[a]Reaction conditions: substrate (50 μmol), catalyst (10 mg), solvent (5 mL), temperature (303 K), N$_2$ (1 atm), Xe lamp (λ >300 nm). [b]Solvents were selected in respect to the solubility of substrates and products. [c]Photoirradiation time. [d]Determined by GC. [e]Catalyst (5 mg). [f]Substrate (25 μmol).

surface Ti^{3+} atoms is proportional to the surface area of catalysts. This implies that rutile TiO_2 with larger surface area contains larger number of surface Ti^{3+} atoms and shows higher catalytic activity. It is, however, well-known that the surface defects also behave as the $e^- - h^+$ recombination centers.[10] Detailed effects of the Ti^{3+} amount and the surface area on the catalytic activity, therefore, still remain to be clarified.

Rutile TiO_2 is also effective for hydrogenation of substituted nitroaromatics. As shown in Table 2, photoirradiation of rutile TiO_2 in 2-PrOH solutions containing nitroaromatics with various substituents produces the corresponding anilines with >94% yields, although P25 TiO_2 shows much lower yields. The rutile system also promotes chemoselective nitro hydrogenation even in the presence of reducible substituents; several kinds of anilines with functional groups are successfully obtained (entries 5, 7, 9, 11, and 13). This is due to the reduction potentials of these substituents being more negative than those of nitro group. As shown in Figure 6, the half-wave reduction potentials of styrene (-2.41 V),[47] benzamide (-2.23 V),[48] benzonitrile (-2.03 V),[49] and benzaldehyde (-1.34 V)[50] are more negative than those of nitrobenzene (0.16 V).[42] This thus enables chemoselective nitro hydrogenation on the photoactivated rutile TiO_2.

CONCLUSION

We found that rutile TiO_2 particles, activated by UV irradiation, promote highly efficient and selective photocatalytic hydrogenation of nitroaromatics with alcohol as a hydrogen source. The surface Ti^{3+} atoms of rutile TiO_2 behave as the adsorption site for nitroaromatics and the trapping site for photoformed conduction band e^-. These two effects facilitate rapid nitro-to-amine hydrogenation while suppressing side reactions. The rutile TiO_2 system enables chemoselective nitro hydrogenation and is carried out with noble metal-free catalyst at room temperature and atmospheric pressure. This process therefore has a potential to be one of the powerful methods for nitro hydrogenation. Despite a number of studies for TiO_2 photocatalysis, there are only a few reports of reactions specifically enhanced on rutile TiO_2.[51−53] The role of surface Ti^{3+} atoms on rutile TiO_2 clarified here may help open a new strategy toward the development of active photocatalysts and new methods for photocatalysis-based organic synthesis.

EXPERIMENTAL SECTION

Preparation of HyCOM TiO_2 (Sample 6). This was prepared according to literature procedure.[54] Titanium *n*-butoxide (5 g) was dissolved in toluene (14 mL) within a glass tube (20 mL), and the tube was set in an autoclave (capacity, 40 mL). Water (5 mL) was added to a gap between the glass tube and the autoclave wall, and the autoclave was purged with N_2. The autoclave was heated to 578 K with a heating rate 2.7 K min^{-1}, and the temperature was held for 8 h. The resulting solid was recovered by filtration, washed thoroughly with water, and dried in vacuo for 12 h, affording HyCOM TiO_2 as white powder.

Preparation of Pt/JRC-TIO-6 (Sample 14). JRC-TIO-6 (200 mg) and $H_2PtCl_6 \cdot H_2O$ (5.2 mg) were added to an aqueous 2-PrOH solution (0.5 M, 10 mL) within a Pyrex glass tube (φ 12 mm; capacity, 20 mL). The tube was sealed with a rubber septum cap. The catalyst was dispersed well by ultrasonication for 5 min, and N_2 was bubbled through the solution for 5 min. The tube was photoirradiated for 50 h at λ >300 nm with magnetic stirring using a 2 kW Xe lamp (USHIO Inc.),[24] where the light intensity at 300−450 nm was 27.3 W m^{-2}. The resulting solid was recovered by filtration, washed thoroughly with water, and dried in vacuo for 12 h, affording Pt/JRC-TIO-6 as gray powder.

Preparation of Ag/JRC-TIO-6 (Sample 15). JRC-TIO-6 (200 mg) and $AgNO_3$ (5.1 mg) were added to an aqueous 2-PrOH solution (0.5 M, 30 mL) within a Pyrex glass tube (φ 35 mm; 50 mL). The tube was purged with N_2 and photoirradiated for 4 h by a Xe lamp. Filtration, washing, and drying affords Ag/JRC-TIO-6 as dark purple powder.

Preparation of Pd/JRC-TIO-6 (Sample 16). JRC-TIO-6 (200 mg) and $Pd(NO_3)_2$ (2.6 mg) were added to a mixture of water (4.4 mL), HNO_3 (0.1 mL), HCl (0.3 mL), and MeOH (25 mL) within a Pyrex glass tube (φ 35 mm; 50 mL). The tube was purged with N_2 and photoirradiated for 6 h by a Xe lamp. Filtration, washing, and drying affords Pd/JRC-TIO-6 as gray powder.

Preparation of Au/JRC-TIO-6 (Sample 17). JRC-TIO-6 (200 mg) and $HAuCl_4 \cdot 4H_2O$ (3.8 mg) were added to MeOH (30 mL) within a Pyrex glass tube (φ 35 mm; 50 mL). The tube was purged with N_2 and photoirradiated for 6 h by a Xe lamp. Filtration, washing, and drying affords Au/JRC-TIO-6 as purple powder.

Photoreaction Procedure. Each nitro compound was dissolved in 2-PrOH solution. The solution and catalyst were added to a Pyrex glass tube (φ 12 mm; capacity, 20 mL), and the tube was sealed with a rubber septum cap. The catalyst was dispersed well by ultrasonication for 5 min, and N_2 was bubbled through the solution for 5 min. The tube was photoirradiated at λ >300 nm with magnetic stirring using a 2 kW Xe lamp (USHIO Inc.), where the light intensity at 300−450 nm was 27.3 W m^{-2}. The solution temperature during photoirradiation was 303 K. After the reaction, the gas phase product was analyzed by GC-TCD. The catalyst was recovered by centrifugation, and the resulting solution was analyzed by GC-FID or HPLC (UV−vis detector). The substrate and product concentrations were calibrated with authentic samples. Analysis was performed at least three times and the errors were $\pm0.2\%$.

Action Spectrum Analysis. The reaction was carried out using a 2-PrOH/toluene (1/9 w/w) mixture (2 mL) containing nitrobenzene (20 μmol) and JRC-TIO-6 TiO_2 (sample **11**, 2 mg) within a Pyrex glass tube (φ 12 mm; capacity, 20 mL). After ultrasonication and N_2 bubbling, the tube was photoirradiated using a Xe lamp for 5 h, where the incident light was monochromated by band-pass glass filters (Asahi Techno Glass Co.). The full-width at half-maximum (fwhm) of the light was 11−16 nm. The photon number entered into the reaction vessel was determined with a spectroradiometer USR-40 (USHIO Inc.).[55]

Analysis. FTIR spectra were measured on a FT/IR 610 system equipped with a DR-600B in situ cell (JASCO Corp.). XPS analysis was performed using a JEOL JPS-9000MX spectrometer with Mg $K\alpha$ radiation as the energy source. Diffuse-reflectance UV−vis spectra were measured on an UV−vis spectrophotometer (JASCO Corp.; V-550 equipped with Integrated Sphere Apparatus ISV-469) with $BaSO_4$ as a reference. Total amounts of metal on the catalysts were determined by an X-ray fluorescence spectrometer (Seiko Instruments Inc.; SEA2110). XRD analysis was carried out on Philips X'Pert-MPD spectrometer.

ASSOCIATED CONTENT

S Supporting Information

XRD patterns for TiO₂ samples (Figure S1), band gap determination of nitrobenzene-adsorbed rutile TiO₂ (Figure S2), diffuse-reflectance UV−vis spectra of TiO₂ samples (Figure S3). This material is available free of charge via the Internet at http://pubs.acs.org.

AUTHOR INFORMATION

Corresponding Author
*E-mail: shiraish@cheng.es.osaka-u.ac.jp.

Notes

The authors declare no competing financial interest.

ACKNOWLEDGMENTS

REFERENCES

(1) Dowing, R. S.; Kunkeler, P. J.; van Bekkum, H. *Catal. Today* **1997**, *37*, 121−136.
(2) Burawoy, A.; Critchley, J. P. *Tetrahedron* **1959**, *5*, 340−351.
(3) Rylander, P. N. *Catalytic Hydrogenation in Organic Synthesis*; Academic Press: New York, 1979; p 122.
(4) Corma, A.; Serna, P.; Concepción, P.; Calvino, J. J. *J. Am. Chem. Soc.* **2008**, *130*, 8748−8753.
(5) Reis, P. M.; Royo, B. *Tetrahedron Lett.* **2009**, *50*, 949−952.
(6) Corma, A.; Serna, P. *Science* **2006**, *313*, 332−334.
(7) Corma, A.; Conceptión, P.; Serna, P. *Angew. Chem., Int. Ed.* **2007**, *46*, 7266−7269.
(8) Boronat, M.; Conceptión, P.; Corma, A.; González, S.; Illas, F.; Serna, P. *J. Am. Chem. Soc.* **2007**, *129*, 16230−16237.
(9) Mitsudome, T.; Mikami, Y.; Matoba, M.; Mizugaki, T.; Jitsukawa, K.; Kaneda, K. *Angew. Chem., Int. Ed.* **2012**, *51*, 136−139.
(10) Hoffmann, M. R.; Martin, S. T.; Choi, W.; Bahnemann, D. W. *Chem. Rev.* **1995**, *95*, 69−96.
(11) Fox, M. A.; Dulay, M. T. *Chem. Rev.* **1993**, *93*, 341−357.
(12) Maldotti, A.; Molinari, A.; Amadelli, R. *Chem. Rev.* **2002**, *102*, 3811−3836.
(13) Palmisano, G.; Augugliaro, V.; Pagliano, M.; Palmisano, L. *Chem. Commun.* **2007**, 3425−3437.
(14) Fagnoni, M.; Dondi, D.; Ravelli, D.; Albini, A. *Chem. Rev.* **2007**, *107*, 2725−2756.
(15) Shiraishi, Y.; Hirai, T. *J. Photochem. Photobiol. C* **2008**, *9*, 157−170.
(16) Palmisano, G.; García-López, E.; Mercí, G.; Loddo, V.; Yurdakal, S.; Augugliaro, V.; Palmisano, L. *Chem. Commun.* **2010**, *46*, 7074−7089.
(17) Mahdavi, F.; Bruton, T. C.; Li, Y. *J. Org. Chem.* **1993**, *58*, 744−746.
(18) Ferry, J. L.; Glaze, W. H. *Langmuir* **1998**, *14*, 3551−3555.
(19) Maldotti, A.; Andreotti, L.; Molinari, A.; Tollari, S.; Penoni, A.; Cenini, S. *J. Photochem. Photobiol. A* **2000**, *133*, 129−133.
(20) Imamura, K.; Iwasaki, S.-i.; Maeda, T.; Hashimoto, K.; Ohtani, B.; Kominami, H. *Phys. Chem. Chem. Phys.* **2011**, *13*, 5114−5119.
(21) Tada, H.; Ishida, T.; Takao, A.; Ito, S. *Langmuir* **2004**, *20*, 7898−7900.
(22) Kiyonaga, T.; Fujii, M.; Akita, T.; Kobayashi, H.; Tada, H. *Phys. Chem. Chem. Phys.* **2008**, *10*, 6553−6561.
(23) Füldner, S.; Mild, R.; Siegmund, H. I.; Schroeder, J. A.; Gruber, M.; König, B. *Green Chem.* **2010**, *12*, 400−406.
(24) Shiraishi, Y.; Sugano, Y.; Tanaka, S.; Hirai, T. *Angew. Chem., Int. Ed.* **2010**, *49*, 1656−1660.
(25) Brezová, V.; Tarábek, P.; Dvoranová, D.; Staško, A.; Biskupič, S. *J. Photochem. Photobiol. A* **2003**, *155*, 179−198.
(26) Tanaka, K.; Capule, M. F. V.; Hisanaga, T. *Chem. Phys. Lett.* **1991**, *187*, 73−76.
(27) Ohtani, B.; Prieto-Mahaney, O. O.; Li, D.; Abe, R. *J. Photochem. Photobiol. A* **2010**, *216*, 179−182.
(28) Ohno, T.; Sarukawa, K.; Matsumura, M. *J. Phys. Chem. B* **2001**, *105*, 2417−2420.
(29) Ramis, G.; Busca, G.; Cristiani, C.; Lietti, L.; Forzatti, P.; Bregani, F. *Langmuir* **1992**, *8*, 1744−1749.
(30) Papageorgiou, A. C.; Beglitis, N. S.; Pang, C. L.; Teobaldi, G.; Cabailh, G.; Chen, Q.; Fisher, A. J.; Hofer, W. A.; Thornton, G. *Proc. Natl. Acad. Sci. U.S.A.* **2010**, *107*, 2391−2396.
(31) Rodriguez, J. A.; Jirsak, T.; Liu, G.; Hrbek, J.; Dvorak, J.; Maiti, A. *J. Am. Chem. Soc.* **2001**, *123*, 9597−9605.
(32) Dohnálek, Z.; Lyubinetsky, I.; Rousseau, R. *Prog. Surf. Sci.* **2010**, *85*, 161−205.
(33) Ahmad, I.; Dines, T. J.; Rochester, C. H.; Anderson, J. A. *J. Chem. Soc., Faraday Trans.* **1996**, *92*, 3225−3231.
(34) Hebenstreit, W.; Ruzycki, N.; Herman, G. S.; Gao, Y.; Diebold, U. *Phys. Rev. B* **2000**, *62*, R16334−R16336.
(35) Diebold, U.; Lehman, J.; Mahmoud, T.; Kuhn, M.; Leonardelli, G.; Hebenstreit, W.; Schmid, M.; Varga, P. *Surf. Sci.* **1998**, *411*, 137−153.
(36) Yang, Y. Z.; Chang, C.-H.; Idriss, H. *Appl. Catal., B* **2006**, *67*, 217−222.
(37) Reiß, S.; Krumm, H.; Niklewski, A.; Staemmler, V.; Wöll, C. *J. Chem. Phys.* **2002**, *116*, 7704−7713.
(38) Cherian, S.; Wamser, C. C. *J. Phys. Chem. B* **2000**, *104*, 3624−3629.
(39) Creutz, C.; Brunschwig, B. S.; Sutin, N. *J. Phys. Chem. B* **2005**, *109*, 10251−10260.
(40) Irie, H.; Kamiya, K.; Shibanuma, T.; Miura, S.; Tryk, D. A.; Yokoyama, T.; Hashimoto, K. *J. Phys. Chem. C* **2009**, *113*, 10761−10766.
(41) Yu, H.; Irie, H.; Shimodaira, Y.; Hosogi, Y.; Kuroda, Y.; Miyauchi, M.; Hashimoto, K. *J. Phys. Chem. C* **2010**, *114*, 16481−16487.
(42) Fan, L.-J.; Wang, C.; Chang, S.; Yang, Y. *J. Electroanal. Chem.* **1999**, *477*, 111−120.
(43) Panayotov, D. A.; Burrows, S. P.; Morris, J. R. *J. Phys. Chem. C* **2012**, *116*, 4535−4544.
(44) Martyanov, I. N.; Klabunde, K. J. *Environ. Sci. Technol.* **2003**, *37*, 3448−3453 ; Φ_{AQY} = 0.1% (at 313 nm), for decomposition of acetaldehyde in water on P25.
(45) McMurray, T. A.; Byrne, J. A.; Dunlop, P. S. M.; McAdams, E. T. *J. Appl. Electrochem.* **2005**, *35*, 723−731 ; Φ_{AQY} = 9% (at 300 nm), for decomposition of formic acid in water on P25.
(46) Ma, C. M.; Wang, W.; Ku, Y.; Jeng, F. T. *Chem. Eng. Technol.* **2007**, *30*, 1083−1087 ; Φ_{AQY} = 4% (at 365 nm), for decomposition of benzene in air on P25.
(47) Dahlén, A.; Nilsson, Å.; Hilmersson, G. *J. Org. Chem.* **2006**, *71*, 1576−1580.
(48) Benedetti, L.; Borsari, M.; Dallari, D.; Fontanesi, C.; Grandi, G.; Gavioli, G. *Electrochim. Acta* **1994**, *39*, 2723−2728.
(49) Romanin, A. M.; Gennaro, A.; Vianello, E. *J. Electroanal. Chem.* **1978**, *88*, 175−185.
(50) Willits, C. O.; Ricciuti., C.; Knight, H. B.; Swern, D. *Anal. Chem.* **1952**, *24*, 785−790.
(51) Jia, J.; Ohno, T.; Matsumura, M. *Chem. Lett.* **2000**, 908−909.
(52) Wang, Y.; Zhang, L.; Deng, K.; Chen, X.; Zou, Z. *J. Phys. Chem. C* **2007**, *111*, 2709−2714.
(53) Yurdakal, S.; Palmisano, G.; Loddo, V.; Augugliaro, V.; Palmisano, L. *J. Am. Chem. Soc.* **2008**, *130*, 1568−1569.
(54) Kominami, H.; Kohno, M.; Takada, Y.; Inoue, M.; Inui, T.; Kera, Y. *Ind. Eng. Chem. Res.* **1999**, *38*, 3925−3931.
(55) Tsukamoto, D.; Shiraishi, Y.; Sugano, Y.; Ichikawa, S.; Tanaka, S.; Hirai, T. *J. Am. Chem. Soc.* **2012**, *134*, 6309−6315.